CHIRAL SU(3) DYNAMICS WITH COUPLED CHANNELS: INCLUSION OF P-WAVE MULTIPOLES

J. Caro Ramon, N. Kaiser, S. Wetzel and W. Weise

Physik-Department, Technische Universität München
Institut für Theoretische Physik, D-85747 Garching, Germany

Abstract

We extend our recent non-perturbative chiral SU(3) coupled channel approach to pion- and photon-induced η- and K-meson production off protons by including all strong and electromagnetic p-wave multipoles. We identify the p-wave amplitudes of the next-to-leading order SU(3) chiral meson-baryon Lagrangian with a coupled channel potential which is iterated to infinite orders in a separable Lippmann-Schwinger equation. Our approach to η- and K-photoproduction introduces no additional free parameters. By adjusting a few finite range parameters and the unknown parameters in the Lagrangian, we are able to simultaneously describe a very large amount of low-energy data. These include the total and differential cross sections of the π-induced reactions $\pi^- p \to \eta n, K^0\Lambda, K^0\Sigma^0, K^+\Sigma^-$ and $\pi^+ p \to K^+\Sigma^+$ as well as those of photoproduction $\gamma p \to \eta p, K^+\Lambda, K^+\Sigma^0, K^0\Sigma^+$. The polarization observables measured in η- and K-photoproduction are particularly sensitive to interference terms between the s- and p-wave multipoles. The total cross section data are remarkably well reproduced in all channels. There remain, however, some open questions concerning details of angular distributions and polarization observables.

Accepted for publication in *Nuclear Physics* **A**.

* *Work supported in part by BMBF and DFG*

1 Introduction

In a recent publication [1] we have developed a theoretical model to study simultaneously pion- and photon-induced production of eta- and K-mesons from protons, based on our previous work in ref.[2]. In contrast to most other approaches [3, 4, 5] we do not introduce explicit (baryonic or mesonic) resonances. Our starting point is the SU(3) chiral effective Lagrangian for the octet baryons $(N, \Lambda, \Sigma, \Xi)$ and the octet pseudoscalar Goldstone bosons (π, K, η) with interactions controlled by chiral symmetry and a low-momentum expansion. In ref.[1] we have identified the s-wave meson-baryon amplitudes generated by the SU(3) chiral Lagrangian with a coupled channel potential matrix which is iterated to infinite order in a separable Lippmann-Schwinger equation in momentum space. The resulting multi-channel S-matrix is automatically unitary, and one naturally obtains cusp effects at secondary thresholds (e.g. at the $K\Sigma$-threshold for reactions with $K\Lambda$-final states). Furthermore, strong attraction is predicted by the SU(3) chiral Lagrangian in certain s-wave channels, namely $\bar{K}N$ with total isospin 0 and $K\Sigma$ with total isospin 1/2. As a consequence, quasi-bound s-wave meson-baryon states emerge in the coupled channel scheme. In fact these states possess all the properties attributed to the baryon resonances $\Lambda(1405)$ and $S_{11}(1535)$ [2]. In particular the unstable $K\Sigma$-bound state has a large branching ratio for decaying into ηN which is the outstanding feature of the nucleon resonance $S_{11}(1535)$.

Remaining adjustable parameters (a priori unknown coefficients in the Lagrangian and short range cut-offs in the separable Lippmann-Schwinger equation) are fixed in a simultaneous fit to a large amount of low energy data. These include the total cross sections for elastic and inelastic K^-p-scattering ($K^-p \to K^-p, \bar{K}^0n, \pi^0\Lambda, \pi^0\Sigma^0, \pi^-\Sigma^+, \pi^+\Sigma^-$) as well as the total cross sections for pion- and photon-induced η- and K-production ($\pi^-p \to \eta n, K^0\Lambda, K^0\Sigma^0, K^+\Sigma^-$ and $\gamma p \to \eta p, K^+\Lambda, K^+\Sigma^0, K^0\Sigma^+$). Among these data the most precise ones are those for $\gamma p \to \eta p$ measured at MAMI [6]. One finds that the combined MAMI/ELSA η-photoproduction total cross sections [6, 7] can be well reproduced in s-wave approximation. On the other hand, for the kaon photoproduction channels $\gamma p \to K^+\Lambda, K^+\Sigma^0$ measured at ELSA [8, 9], the s-wave approximation works only in the near threshold region. At higher energies s-waves alone considerably underestimate the total cross sections and evidently p-waves start to become important. This is also seen from the angular distributions of the differential cross section which are no longer isotropic at these energies. Furthermore, the Λ- and Σ-recoil polarizations measured at ELSA [8] (via the self-analyzing weak decay of these hyperons) can result only from s- and p-wave interference terms. Also, existing differential cross sections for pion-induced η- and K-production point toward the importance of the meson-baryon p-wave amplitudes.

The purpose of this work is to extend our previous coupled channel framework [1, 2] by including, in a systematic manner, the strong interaction $p_{1/2}$- and $p_{3/2}$-partial wave amplitudes together with the photoproduction p-wave multipoles (E_{1+}, M_{1+}, M_{1-}). The latter correspond to the electric quadrupole transition (E_{1+}) and the magnetic dipole transitions $(M_{1\pm})$ in pseudoscalar meson photoproduction. In complete analogy with the treatment of the s-waves in ref.[1] we will identify the (strong and electromagnetic) p-wave multipoles given by the first and second order SU(3) chiral meson-baryon Lagrangian with a coupled channel potential. This matrix of driving terms is iterated to infinite orders in a separable (p-wave) Lippmann-Schwinger equation using the same values of the short range cut-offs as for the s-waves. For the strong meson-baryon interaction seven new parameters come along with four spin-non-flip terms and three spin-flip terms at next-to-leading order.

A very welcome feature of our approach is that the inclusion of the electromagnetic interaction (η and K-photoproduction) is completely parameterfree. The respective p-wave

multipoles (E_{1+}, M_{1+}, M_{1-}) depend only on well known baryon magnetic moments and the SU(3) axial vector coupling constant F and D. It is then quite non-trivial to achieve a good description of so many empirical photon- and pion-induced data within a coupled channel approach, based on a single chiral effective Lagrangian, in which all these processes are correlated.

In this paper we do not aim for an accurate reproduction of elastic πN-phase shifts. This is a drawback of the present approach which could be fixed by parametrizing the relevant πN-amplitudes. Our goal here is rather to focus on the impact of chiral $SU(3)_L \times SU(3)_R$ on hadron dynamics involving kaons and η-mesons. The more detailed influence of the elastic πN-channel will be investigated at a later stage.

On the experimental side there are now improved data (total and differential cross sections and hyperon recoil polarizations) for kaon photoproduction from ELSA [9, 10]. In the case of η-photoproduction the polarized photon asymmetry has recently been measured at GRAAL [11], and the polarized target asymmetry was measured at ELSA [12]. At Brookhaven there is an ongoing program [13] to measure $\pi^- p \to \eta n$ and related reactions.

This paper is organized as follows. In section 2 we present the formalism to calculate the strong and electromagnetic p-wave amplitudes within our approach. We first display the relevant p-wave part of the SU(3) chiral meson-baryon Lagrangian at second order, derive expressions for the strong p-wave potentials and formulate the separable p-wave Lippmann-Schwinger equation. Next we apply the same formalism to η- and K-photoproduction and give expressions for the observables (total and differential cross sections as well as the polarized target asymmetry, the recoil polarization and the polarized photon asymmetry) in s- and p-wave approximation. In section 3 we discuss in detail our results for pion- and photon-induced η- and K-meson production off protons, and we conclude in section 4 with a summary.

2 Formalism

2.1 Chiral effective Lagrangian

The leading order relativistic SU(3) chiral meson-baryon Lagrangian and the s-wave part at next-to-leading order have already been developed and explained in detail in section 2.1 of ref.[1]. Therefore we display here only the new terms relevant to p-wave meson-baryon scattering at second order in small momenta [14]:

$$\begin{aligned}\mathcal{L}^{(2)}_{\phi B} &= 2g_D\,\mathrm{tr}(\overline{B}\{\vec{u}\cdot\vec{u},B\}) + 2g_F\,\mathrm{tr}(\overline{B}[\vec{u}\cdot\vec{u},B]) + 2g_0\,\mathrm{tr}(\overline{B}B)\,\mathrm{tr}(\vec{u}\cdot\vec{u}) \\ &\quad +2g_1\,\mathrm{tr}(\overline{B}\vec{u})\cdot\mathrm{tr}(\vec{u}B) + 2h_D\,\mathrm{tr}(\overline{B}i\vec{\sigma}\cdot\{\vec{u}\times\vec{u},B\}) + 2h_F\,\mathrm{tr}(\overline{B}i\vec{\sigma}\cdot[\vec{u}\times\vec{u},B]) \\ &\quad +2h_1\,\mathrm{tr}(\overline{B}i\vec{\sigma}\times\vec{u})\cdot\mathrm{tr}(\vec{u}B). \qquad (1)\end{aligned}$$

Here, the SU(3)-matrix B represents the octet baryons $(N, \Lambda, \Sigma, \Xi)$. The axial vector quantity $u^\mu = -\partial^\mu\phi/2f$ is proportional to the gradient of the octet pseudoscalar meson fields (π, K, η) represented by the SU(3)-matrix ϕ and $f = 92.4$ MeV denotes the pion decay constant, $\vec{\sigma}$ is the usual spin-vector given by the 2×2 Pauli-matrices. Note that in flavor SU(3) there are four independent non-spin-flip terms with coefficients g_D, g_F, g_0, g_1 and three independent spin-flip terms with coefficients h_D, h_F, h_0. Further possible SU(3)-symmetric p-wave interaction terms at this order can be expressed through the ones given in eq.(1) using non-trivial trace relations [14].

When computing the photoproduction p-wave multipoles at a later stage, we will need the photon-baryon vertex at next-to-leading order, i.e. the terms proportional to baryon

anomalous magnetic moments. In SU(3) the corresponding part of the Lagrangian reads

$$\mathcal{L}^{(2)}_{\gamma B} = \frac{1}{2M_0}\mathrm{tr}\Big(\overline{B}\vec{\sigma}\cdot(\vec{\nabla}\times\vec{A})(\kappa_D\{Q,B\}+\kappa_F[Q,B])\Big)\,, \tag{2}$$

where $\vec{A}$ denotes the usual electromagnetic vector potential, $Q = \frac{1}{3}\mathrm{diag}(2,-1,-1)$ is the quark charge matrix and $M_0 \simeq 0.9$ GeV the octet baryon mass in the chiral limit [15]. In the chiral limit (of vanishing quark masses $m_u = m_d = m_s = 0$) the baryon anomalous magnetic moments are related to the two constants κ_D and κ_F in eq.(2) as follows,

$$\begin{aligned}
&\kappa_p = \frac{1}{3}\kappa_D + \kappa_F = 1.79, \quad \kappa_n = -\frac{2}{3}\kappa_D = -1.91, \quad \kappa_\Lambda = -\frac{1}{3}\kappa_D = -0.61,\\
&\kappa_{\Sigma^+} = \frac{1}{3}\kappa_D + \kappa_F = 1.46, \quad \kappa_{\Sigma^0} = \frac{1}{3}\kappa_D = 0.65, \quad \kappa_{\Lambda\Sigma^0} = \frac{1}{\sqrt{3}}\kappa_D = 1.61,
\end{aligned} \tag{3}$$

However, as the empirical values given in eq.(3) indicate, there are significant deviations from the simple SU(3)-relations. To be more accurate at this point, we will actually use the empirical values of the baryon anomalous magnetic moments inasmuch as they are available. The empirically unknown κ_{Σ^0} and the sign of the transition magnetic moment $\kappa_{\Lambda\Sigma^0}$ are taken in eq.(3) from the recent chiral perturbation theory calculation of ref.[16]. This completes the discussion of the p-wave extension of the chiral effective Lagrangian. The seven unknown parameters $g_D, g_F, g_0, g_1, h_D, h_F, h_1$ will be fixed in a fit to many scattering data in section 3.

2.2 Coupled channel approach

Let us now describe the coupled channel approach to the strong (p-wave) meson-baryon interaction. We label the meson-baryon states $|\pi N\rangle$, $|\eta N\rangle$, $|K\Lambda\rangle$, $|K\Sigma\rangle$ with total isospin $I = 1/2$ and the states $|\pi N\rangle$, $|K\Sigma\rangle$ with total isospin $I = 3/2$ by an index which runs from 1 to 6, in that order. In a specific channel the meson center-of-mass energy E_ϕ is given by

$$E_\phi = \frac{s - M_B^2 + m_\phi^2}{2\sqrt{s}}\,, \tag{4}$$

where $\sqrt{s}$ is the total center-of-mass energy of the meson-baryon system and M_B, m_ϕ denote the mass of the corresponding baryon and meson. The center-of-mass momentum in channel j reads

$$k_j = \sqrt{E_\phi^2 - m_\phi^2} = i\sqrt{m_\phi^2 - E_\phi^2}\,, \tag{5}$$

and we have also given its analytical continuation below threshold (i.e. for $E_\phi < m_\phi$).

Because of the spin-orbit interaction there are two different p-wave amplitudes in meson-baryon scattering (corresponding to the $p_{1/2}$- and $p_{3/2}$-states), and these do not mix. In both angular momentum states the different channels are coupled through a (reduced) p-wave potential in momentum space,

$$V_{ij}^{(1\mp)} = \frac{\sqrt{M_i M_j}}{4\pi f^2\sqrt{s}}\, C_{ij}^{(1\mp)}\,, \tag{6}$$

where we have taken away the characteristic p-wave factor $k_i k_j$ which will appear explicitly in the coupled channel equation. The relative coupling strengths $C_{ij}^{(1\mp)}$ are calculated from the chiral SU(3) meson-baryon Lagrangian at next-to-leading order. Explicit expressions for

these coupling strengths and a discussion of various contributions can be found in appendix A .

In the next step the potential $V_{ij}^{(1\mp)}$ is iterated to all orders in a separable Lippmann-Schwinger equation of the form

$$k_i \widetilde{T}_{ij}^{(1\mp)} k_j = k_i V_{ij}^{(1\mp)} k_j + \sum_n \int \frac{d^3 l}{2\pi^2} \frac{1}{k_n^2 + i0 - l^2} \Big(\frac{\alpha_n^2 + k_n^2}{\alpha_n^2 + l^{\,2}} \Big)^4 k_i V_{in}^{(1\mp)} l_n \, l_n \widetilde{T}_{nj}^{(1\mp)} k_j \, . \qquad (7)$$

The resulting multi-channel p-wave T-matrix is $T_{ij}^{(1\mp)} = k_i \widetilde{T}_{ij}^{(1\mp)} k_j$. The separable Lippmann-Schwinger equation can be solved analytically by simple matrix inversion,

$$T_{ij}^{(1\pm)} = k_i \Big[\Big(1 - V^{(1\pm)} \cdot G^{(1)} \Big)^{-1} \cdot V^{(1\pm)} \Big]_{ij} k_j \, , \qquad (8)$$

where $G^{(1)}$ is the diagonal matrix with elements

$$G_n^{(1)} = \frac{2}{\pi} \int_0^\infty \frac{dl \, l^4}{k_n^2 + i0 - l^2} \Big(\frac{\alpha_n^2 + k_n^2}{\alpha_n^2 + l^2} \Big)^4 = \frac{k_n^2 - \alpha_n^2}{16 \alpha_n^3} (\alpha_n^4 + 10 \alpha_n^2 k_n^2 + k_n^4) - i \, k_n^3 \, , \qquad (9)$$

and the center-of-mass momentum k_n in the intermediate state n is given by eq.(3) together with its analytical continuation below threshold. Note that we are using here the same values for the short range cut-offs α_n as for the s-waves in ref.[1]. The exponent on the off-shell form factor $[(\alpha_n^2 + k_n^2)/(\alpha_n^2 + l^2)]^4$ follows from the general rule $2L+2$ for given orbital angular momentum L [17]. The resulting multi-channel p-wave S-matrix $S_{ij}^{(1\mp)} = \delta_{ij} - 2i \sqrt{k_i k_j} \, T_{ij}^{(1\mp)}$ is exactly unitarity in the subspace of the kinematically open channels.

Note that in the sense of chiral (i.e. small momentum) counting the iterations generated by the separable Lippmann-Schwinger equation do not affect the leading order current-algebra results for s-waves [1, 2]. In the p-wave channels, the formal chiral power counting is distorted by the short distance cut-off scale α_n in eq.(7). It should be pointed out that the KY and ηN channels investigated in this work have dynamic features quite different from those familiar from near threshold πN scattering. In particular there is no primary reason to expect that leading order current-algebra results would be relevant at the much higher energy (around 1 GeV) involved in KY- and ηN-production. The main purpose of our investigation is to explore to what extent chiral $SU(3)_L \times SU(3)_R$ still plays a significant role in constraining the driving terms $V_{ij}^{(1\mp)}$ in the Lippmann-Schwinger equation eq.(7).

In order to calculate observables for π-induced η- and K-meson production one first has to relate the corresponding (s- and p-wave) T-matrix elements to the ones defined in the isospin-basis. One finds for the physical reaction channels,

$$\begin{aligned}
\pi^- p \to \eta n : \qquad & \frac{\sqrt{6}}{3} T_{12}^{(l\mp)} \, , \\
\pi^- p \to K^0 \Lambda : \qquad & \frac{\sqrt{6}}{3} T_{13}^{(l\mp)} \, , \\
\pi^- p \to K^0 \Sigma^0 : \qquad & \frac{\sqrt{2}}{3} \Big[T_{56}^{(l\mp)} - T_{14}^{(l\mp)} \Big] \, , \\
\pi^- p \to K^+ \Sigma^- : \qquad & \frac{1}{3} \Big[2 T_{14}^{(l\pm)} + T_{56}^{(l\pm)} \Big] \, , \\
\pi^+ p \to K^+ \Sigma^+ : \qquad & T_{56}^{(l\pm)} \, , \qquad (10)
\end{aligned}$$

and the superscript (0+) refers to the s-wave amplitudes which have already been calculated in ref.[1]. For each specific reaction channel the differential cross section reads

$$\frac{d\sigma}{d\Omega} = \frac{k_{\rm out}}{k_{\rm in}} \Big\{ |T^{(0+)} + z \, (2T^{(1+)} + T^{(1-)})|^2 + (1 - z^2) |T^{(1+)} - T^{(1-)}|^2 \Big\} \, , \qquad (11)$$

with $z = \cos\theta$ the cosine of the center-of-mass scattering angle θ, and we have omitted the indices $i, j \in \{1, \ldots 6\}$. The prefactor $k_{\rm out}/k_{\rm in}$ is the usual flux and two-body phase-space factor. Obviously, the angular distribution of the differential cross section is restricted to a quadratic polynomial (of $z = \cos\theta$) in s- and p-wave approximation. The total cross section for a specific reaction channel is finally calculated as

$$\sigma_{\rm tot} = 4\pi \frac{k_{\rm out}}{k_{\rm in}} \Big\{ |T^{(0+)}|^2 + 2|T^{(1+)}|^2 + |T^{(1-)}|^2 \Big\} \,. \tag{12}$$

2.3 Meson photoproduction

We now extend the same formalism to p-wave meson photoproduction. As in ref.[1] our basic assumption is that the photoproduction can be described by a Lippmann-Schwinger equation. In complete analogy with the strong interaction part we identify the p-wave photoproduction potentials (named generically B_j) with the electric quadrupole amplitude E_{1+} and the magnetic dipole amplitudes $M_{1\pm}$ calculated from the next-to-leading order chiral effective Lagrangian. For the description of the photoproduction reaction $\gamma p \to \eta p, K^+\Lambda, K^+\Sigma^0, K^0\Sigma^+$ we have to know the p-wave photoproduction potential B_j for $\gamma p \to \phi B$, where ϕB refers to the meson-baryon states with total isospin $I = 1/2$ or $I = 3/2$ and isospin projection $I_3 = +1/2$. In section 2.2 these states have been labeled by an index running from 1 to 6. Leaving out the typical p-wave factor k_j one finds for the reduced p-wave photoproduction potentials,

$$\begin{aligned}
B_1 &= \frac{eM_N}{8\pi f\sqrt{3s}}(D+F)\Big\{2X_\pi(\kappa_n) + Y_\pi(\kappa_p)\Big\} \,, \\
B_2 &= \frac{eM_N}{8\pi f\sqrt{3s}}(3F-D)\, Y_\eta(\kappa_p) \,, \\
B_3 &= \frac{e\sqrt{M_N M_\Lambda}}{8\pi f\sqrt{3s}}\Big\{(-D-3F)X_K(\kappa_\Lambda) + (F-D)\frac{\kappa_{\Lambda\Sigma^0}\,\beta}{2\sqrt{3}M_0}\Big\} \,, \\
B_4 &= \frac{e\sqrt{M_N M_\Sigma}}{8\pi f\sqrt{3s}}\Big\{(D-F)\Big[X_K(\kappa_{\Sigma^0}) + 2Y_K(\kappa_{\Sigma^+})\Big] + (D+3F)\frac{\kappa_{\Lambda\Sigma^0}\,\beta}{6\sqrt{3}M_0}\Big\} \,, \\
B_5 &= \frac{eM_N}{4\pi f\sqrt{6s}}(D+F)\Big\{Y_\pi(\kappa_p) - X_\pi(\kappa_n)\Big\} \,, \\
B_6 &= \frac{e\sqrt{M_N M_\Sigma}}{4\pi f\sqrt{6s}}\Big\{(D-F)\Big[X_K(\kappa_{\Sigma^0}) - Y_K(\kappa_{\Sigma^+})\Big] + (D+3F)\frac{\kappa_{\Lambda\Sigma^0}\,\beta}{6\sqrt{3}M_0}\Big\} \,.
\end{aligned} \tag{13}$$

These formulae apply separately to the three p-wave multipoles: E_{1+}, M_{1-} and M_{1+}. In these three cases the functions $Y_\phi(\kappa_+)$ (depending on the anomalous magnetic moment κ_+ of a positively charged baryon) and the functions $X_\phi(\kappa_0)$ (depending on the magnetic moment κ_0 of a neutral baryon) represent different expressions. If the photoproduced pseudoscalar meson is neutral the functions $Y_\phi(\kappa_+)$ stand for

$$\begin{aligned}
Y_\phi[E_{1+}](\kappa_+) &= 0 \,, \\
Y_\phi[M_{1-}](\kappa_+) &= -\frac{4+3\kappa_p+\kappa_+}{6M_0} \,, \\
Y_\phi[M_{1+}](\kappa_+) &= \frac{1+\kappa_+}{3M_0} \,,
\end{aligned} \tag{14}$$

and the argument in the square bracket indicates the p-wave multipole under consideration. In the case that the photoproduced meson is positively charged the functions $X_\phi(\kappa_0)$ read

$$\begin{aligned}
X_\phi[E_{1+}](\kappa_0) &= \frac{1}{12(E_\phi^2-m_\phi^2)}\Big\{E_\phi-\frac{4m_\phi^2}{E_\phi}-\frac{m_\phi^2}{M_0}\Big(1+\frac{2m_\phi^2}{E_\phi^2}\Big)+3\Big(1+\frac{m_\phi^2}{M_0E_\phi}\Big)L_\phi\Big\}\,,\\
X_\phi[M_{1-}](\kappa_0) &= \frac{1}{2(E_\phi^2-m_\phi^2)}\Big\{E_\phi+\frac{m_\phi^2-E_\phi^2}{3M_0}(3+3\kappa_p+\kappa_0)-L_\phi\Big\}\,,\\
X_\phi[M_{1+}](\kappa_0) &= \frac{1}{4(E_\phi^2-m_\phi^2)}\Big\{-E_\phi+\frac{4\kappa_0}{3M_0}(E_\phi^2-m_\phi^2)+L_\phi\Big\}\,, \qquad (15)
\end{aligned}$$

with

$$L_\phi=\frac{m_\phi^2}{\sqrt{E_\phi^2-m_\phi^2}}\ln\frac{E_\phi+\sqrt{E_\phi^2-m_\phi^2}}{m_\phi}=\frac{m_\phi^2}{\sqrt{m_\phi^2-E_\phi^2}}\arccos\frac{E_\phi}{m_\phi}\,. \qquad (16)$$

The logarithmic function L_ϕ (together with its analytical continuation below threshold) stems from the meson pole diagram in which the photon couples to the positively charged meson (i.e. a π^+ or a K^+). In eq.(13) there are further contributions from the electromagnetic $\Sigma^0\to\Lambda\gamma$ transition proportional to the transition magnetic moment $\kappa_{\Lambda\Sigma^0}=1.61$. The corresponding weight factor β is different for the three p-wave multipoles and takes the values,

$$\beta[E_{1+}]=0\,,\quad \beta[M_{1-}]=1\,,\quad \beta[M_{1+}]=-2\,. \qquad (17)$$

This concludes the description of the p-wave photoproduction potentials derived from the next-to-leading order SU(3) chiral Lagrangian. One finds that the pertinent expressions depend only on the SU(3) axial vector coupling constant $D\simeq 0.76$ and $F\simeq 0.50$ and known baryon magnetic moments.

Infinitely many rescatterings of the photoproduced meson-baryon state due to the p-wave strong interaction are summed up via the Lippmann-Schwinger equation. The full p-wave photoproduction multipoles (commonly denoted by $\mathcal{M}\in\{E_{1+},M_{1-},M_{1+}\}$) are then given by

$$\mathcal{M}_i=k_i\sum_j\Big[\Big(1-V^{(1\pm)}\cdot G^{(1)}\Big)^{-1}\Big]_{ij}B_j\,, \qquad (18)$$

where the indices $i,j\in\{1,\ldots,6\}$ refer to the isospin-basis. From angular momentum conservation it is clear that the strong interaction $p_{3/2}$-potentials $V_{ij}^{(1+)}$ are the relevant ones for E_{1+} and M_{1+}, whereas M_{1-} is iterated up by the $p_{1/2}$-potential $V_{ij}^{(1-)}$.

Next, we have to express the multipoles for the four physical photoproduction channels by the ones defined in the isospin-basis. One finds,

$$\begin{aligned}
\gamma p\to\eta p: &\qquad \mathcal{M}_2\,,\\
\gamma p\to K^+\Lambda: &\qquad \mathcal{M}_3\,,\\
\gamma p\to K^+\Sigma^0: &\qquad (\sqrt{2}\mathcal{M}_6+\mathcal{M}_4)/\sqrt{3}\,,\\
\gamma p\to K^0\Sigma^+: &\qquad (\sqrt{2}\mathcal{M}_4-\mathcal{M}_6)/\sqrt{3}\,. \qquad (19)
\end{aligned}$$

In order to express the observables of meson photoproduction it is advantageous to use the following linear combinations of three p-wave multipoles,

$$\begin{aligned}
P_1 &= 3E_{1+}+M_{1+}-M_{1-}\,,\\
P_2 &= 3E_{1+}-M_{1+}+M_{1-}\,,\\
P_3 &= 2M_{1+}+M_{1-}\,. \qquad (20)
\end{aligned}$$

In terms of these and the s-wave multipole E_{0+} (see ref.[1]) the differential cross section takes the form,

$$\frac{d\sigma}{d\Omega} = \frac{k_{\rm out}}{k_\gamma}\Big\{|E_{0+} + z\,P_1|^2 + \frac{1}{2}(1-z^2)\Big(|P_2|^2 + |P_3|^2\Big)\Big\}\,, \tag{21}$$

with $k_\gamma = (s - M_N^2)/2\sqrt{s}$ the center-of-mass photon energy and $z = \cos\theta$ the cosine of the center-of-mass scattering angle θ. Again, the angular distributions of the differential cross sections are restricted to a quadratic polynomial (of $z = \cos\theta$) in s- and p-wave approximation. After angular integration one gets the total meson photoproduction cross sections as

$$\sigma_{\rm tot} = 4\pi\frac{k_{\rm out}}{k_\gamma}\Big\{|E_{0+}|^2 + \frac{1}{3}\Big(|P_1|^2 + |P_2|^2 + |P_3|^2\Big)\Big\}\,. \tag{22}$$

Of particular interest are the polarization observables since they vanish identically in pure s-wave approximation. The final state baryon emerges from the photoproduction process with a certain recoil polarization. This means that the probabilities for the baryon spin pointing downward or upward from the reaction plane spanned by the momenta of the photon and the meson are not equal. In the case of kaon photoproduction the recoil polarization Π_r of the hyperons $\Lambda, \Sigma^{0,+}$ is experimentally accessible through their self-analyzing weak decays (into πN). In s- and p-wave approximation the recoil polarization is calculated as follows from the multipoles:

$$\Pi_r = \frac{\sqrt{1-z^2}\,{\rm Im}[(E_{0+} + z\,P_1)(P_2 + P_3)^*]}{|E_{0+} + z\,P_1|^2 + \frac{1}{2}(1-z^2)(|P_2|^2 + |P_3|^2)}\,. \tag{23}$$

Another asymmetry can be measured by using a polarized proton target with the proton spin pointing either parallel or anti-parallel to the normal on the reaction plane. In s- and p-wave approximation the polarized target asymmetry reads

$$A_t = \frac{\sqrt{1-z^2}\,{\rm Im}[(E_{0+} + z\,P_1)(P_3 - P_2)^*]}{|E_{0+} + z\,P_1|^2 + \frac{1}{2}(1-z^2)(|P_2|^2 + |P_3|^2)}\,. \tag{24}$$

Finally, one can produce the meson with linearly polarized photon beams whose polarization vector is either perpendicular or parallel to the reaction plane. The corresponding polarized photon asymmetry reads in s- and p-wave approximation

$$\Sigma_\gamma = \frac{(1-z^2)\,(|P_3|^2 - |P_2|^2)}{2|E_{0+} + z\,P_1|^2 + (1-z^2)(|P_2|^2 + |P_3|^2)}\,. \tag{25}$$

It is clear from eqs.(23,24,25), that even just the signs of the polarization observables $\Pi_r, A_t, \Sigma_\gamma$ already contain non-trivial dynamical information.

3 Results

First, we have to fix parameters. As outlined in the previous section we are working in the isospin-basis and we are using for the meson and baryon masses $m_\pi = 139.57$ MeV, $m_K = 493.65$ MeV, $m_\eta = 547.45$ MeV, $M_N = 938.27$ MeV, $M_\Lambda = 1115.63$ MeV and $M_\Sigma = 1192.55$ MeV. This is a choice which averages out most isospin breaking effects. We keep the values of the axial vector coupling constants $D = 0.782$, $F = 0.485$, and those of the two chiral symmetry breaking parameters $b_D = 0.066$ GeV^{-1}, $b_F = -0.231$ GeV^{-1}

unchanged from ref.[1]. In this work we identify M_0 with the octet baryon mass in the SU(3) chiral limit (of vanishing u-, d- and s-quark mass) and we use $M_0 = 869$ MeV as obtained in a best fit to the data. This value of M_0 is consistent with $M_0 = (0.77 \pm 0.11)$ GeV of ref.[15] as found in a recent heavy baryon chiral perturbation theory calculation to order q^4. The third chiral symmetry breaking parameter b_0 is then determined through the (leading order) mass relation $M_N = M_0 + 4m_K^2(b_F - b_D - b_0) - 2m_\pi^2(b_0 + 2b_F)$ as $b_0 = -0.320$ GeV^{-1}. Such a value of b_0 leads to a relative scalar strangeness content in the nucleon of $y = 0.1$ and to a pion-nucleon sigma-term of $\sigma_{\pi N} = 31$ MeV. Whereas y is compatible with the present empirical determination $y = 0.2 \pm 0.2$ [19], the pion-nucleon sigma-term is somewhat too small compared to the empirical value $\sigma_{\pi N} = (45 \pm 8)$ MeV of [19]. As mentioned already in [1], if one stays to linear order in the quark masses, as done here, then both pieces of information (y and $\sigma_{\pi N}$) cannot be explained by a single value of b_0.

The remaining parameters are adjusted in a best fit to a large amount of pion- and photon-induced data. The four range parameters are found as

$$\alpha_{\pi N} = 480\,\mathrm{MeV}\,, \quad \alpha_{\eta N} = 663\,\mathrm{MeV}\,, \quad \alpha_{K\Lambda} = 1362\,\mathrm{MeV}\,, \quad \alpha_{K\Sigma} = 785\,\mathrm{MeV}\,. \tag{26}$$

We give here sufficiently many digits to make the numerical results reproducible. One observes that the four range parameters are rather close to the values found in [1] where only s-wave amplitudes have been considered, and they are all located in the physically reasonable range $0.5 \ldots 1.4$ GeV. At the same time the coefficients of the four double-derivative s-wave terms come out as

$$d_D = 0.512\,, \quad d_F = -0.509\,, \quad d_0 = -0.996\,, \quad d_1 = 0.173\,, \tag{27}$$

(in units of GeV^{-1}) and those of the four analogous spin-non-flip p-wave terms as

$$g_D = 0.320\,, \quad g_F = 0.026\,, \quad g_0 = -1.492\,, \quad g_1 = 1.452\,. \tag{28}$$

Furthermore, the coefficients of the three spin-flip p-wave terms are found as

$$h_D = 0.778\,, \quad h_F = -0.029\,, \quad h_1 = 0.130\,, \tag{29}$$

(again in units of GeV^{-1}). Note that all these coefficients are of "natural" size. One also observes that the coefficients $d_{D,F,0,1}$ do not differ much from those found in our previous work [1] where only s-wave amplitudes have been considered. In essence, the relative weights between the total cross sections in the different hadronic channels already fix the whole pattern of s-wave amplitudes and their parameters. The addition of p-waves does not change this pattern qualitatively. We have furthermore checked that an equally good description of the $K^- p \to K^- p, \bar{K}^0 n, \pi^0\Lambda, \pi^+\Sigma^-, \pi^0\Sigma^0, \pi^+\Sigma^-$ low-energy data as in ref.[1] can be obtained with the (slightly modified) s-wave parameters eq.(27) after readjusting the range parameters $\alpha_{\bar{K}N}, \alpha_{\pi\Lambda}$ and $\alpha_{\pi\Sigma}$.

Before presenting results for the observables of pion- and photon-induced η- and K-production we like to mention some generic features of our approach. We found that the second order s- and p-wave terms (proportional to $b_{D,F,0}, d_{D,F,0,1}, g_{D,F,0,1}, h_{D,F,1}$) are essential in order to obtain a good fit of the total cross sections for pion-induced η- and K-production. This is quite different from the case of K^--proton elastic and inelastic scattering, where one can obtain a good description of the low energy data already with the leading order terms alone in the coupled channel scheme [20], at the expense of readjusting the pseudoscalar decay constant. Furthermore, we have observed that the baryon anomalous magnetic moments κ_B (collected in eq.(3)) are very important in order to get a good simultaneous

reproduction of the η- and K-photoproduction total cross sections. Setting all κ_B equal to zero would lead to a strong reduction of the magnetic p-wave multipoles $M_{1\pm}$ for kaon-photoproduction which however turn out to be important in the energy region somewhat above threshold. We have also performed a fit taking into account the SU(3) symmetry breaking in the pseudoscalar decay constants by setting $f = f_\pi = 92.4$ MeV for pions, $f = f_K = 113.0$ MeV [21] for kaons and $f = f_\eta = 92.6$ MeV [21] for the η-meson. (Note that we are identifying throughout the physical η-meson with the flavor state η_8.). We find that such SU(3)-breaking effects can be balanced by a slight change of the coefficients of the second order terms and the range parameters. The fit with a single $f = 92.4$ MeV is practically indistinguishable from a fit with three different pseudoscalar decay constants. Therefore we stay with a single $f = 92.4$ MeV as in our previous publications on this and related subjects.

We have also performed systematic searches in which the range parameters α_n (see eq.(9)) entering the p-wave amplitudes were allowed to differ from those of the s-waves. The resulting improvements were only marginal, however, so that the introduction of four more parameters did not appear justified and we stayed with the set eq.(26). Let us now discuss the comparison with the data in detail.

Note that a direct comparison of our s- and p-wave coupled channel model with elastic πN-scattering in the energy range of interest here ($1.5\,\mathrm{GeV} \leq \sqrt{s} \leq 2.0\,\mathrm{GeV}$) would not be meaningful since partial waves of much higher angular momentum and several nucleon resonances contribute in that channel. Introducing πN resonances ($S_{11}(1650)$ etc.) would certainly improve the situation, but at the expense of additional free parameters. In the present paper we have ignored such explicit resonance contributions as well as the coupling to the inelastic $\pi\pi N$ continuum. Deficiencies of the present results for ηN- and KY-production may point to the influence of these neglected effects and should be further explored.

3.1 Total cross sections for π-induced η- and K-production

In Fig.1, we show our results for the total cross sections for pion-induced η- and K-production: $\pi^- p \to \eta n, K^0\Lambda, K^0\Sigma^0, K^+\Sigma^-$ and $\pi^+ p \to K^+\Sigma^+$. The data are taken from the compilation [22]. The agreement of the coupled channel calculation including s- and p-wave amplitudes with the existing data is very good, even for energies considerably above threshold (i.e. up to $p_{\pi,lab} \simeq 2$ GeV). The contributions of the s-wave amplitude and the two p-wave amplitudes to the total cross section are shown separately for each reaction channel. With the inclusion of the p-wave one is now able to describe also the data in the (pure isospin-3/2) channel $\pi^+ p \to K^+\Sigma^+$ up to $p_{\pi,lab} = 1.4$ GeV. In this channel the s-wave contributes very little, as already found in our previous work [1], and the p-wave contribution is completely dominant. Furthermore, with the inclusion of p-wave amplitudes one can describe the total cross section data for $\pi^- p \to K^+\Sigma^-$ up to $p_{\pi,lab} = 1.8$ GeV whereas the s-wave approximation starts to break down around $p_{\pi,lab} = 1.2$ GeV. Note that the large η-production cross section in $\pi^- p \to \eta n$ near threshold (usually interpreted in terms of the nucleon resonance $S_{11}(1535)$ having a large branching ratio into ηN) is still dominated by the s-wave amplitude. In the present approach a s-wave quasi-bound $K\Sigma$-state is formed through the coupled channel dynamics. Furthermore, the peak in the $\pi^- p \to K^0\Lambda$ total cross section is generated by a strong s-wave cusp effect at the $K\Sigma$-threshold as already found in our previous work [1]. As a byproduct of this calculation we extract the complex ηN scattering length $a_{\eta N} = (0.32 + 0.25\,i)$ fm. Whereas its imaginary part agrees with the recent empirical determination $a_{\eta N} = ((0.72 \pm 0.03) + (0.26 \pm 0.03)\,i)$ fm of [23], its real part is about a factor two too small. As mentioned in [23] the real part $\mathrm{Re}\, a_{\eta N}$ cannot exceed

0.4 fm as long as only one S_{11}-resonance is included (as it is the case here) and therefore the relatively small real part is just consistent with this.

Altogether it is highly non-trivial to produce the pattern of relative weights of s- and p-waves as shown in Fig.1. In a coupled channel calculation all reactions get linked together and changes in one channel will immediately affect all the others.

3.2 Differential cross sections for π-induced η- and K-production

In Fig.2 we show some typical examples of angular distributions of the differential cross sections for pion-induced η- and K-production. For the reaction $\pi^- p \to \eta n$ with data taken from [24] one finds that the trend of the data is roughly reproduced, however, with too much deviation from isotropy. In the case $\pi^- p \to K^+\Sigma^-$ (data are taken from [27]) one finds a good reproduction of the angular distribution at low energies. However, moving up in energy the forward-backward asymmetry develops in a way opposite to the data. This means that the magnitudes of the s- and p-wave amplitudes in this channel are given correctly but their interference term has the wrong sign. The same features apply to the channel $\pi^- p \to K^0\Lambda$ where the data stem from [25]. It may be that introduction of the $S_{11}(1650)$-resonance coupling to $K\Lambda$ (and possibly to $K\Sigma$) is necessary here. Merely adding a $S_{11}(1650)$-resonance contribution to the present coupled channel amplitudes did not turn out to be successful since in the fit it affects too much the s-wave amplitudes of the other (strong and electromagnetic) channels. The situation is better for the reaction $\pi^- p \to K^0\Sigma^0$ as can be seen in Fig.2. Here the features of the data (taken from [26]) are well reproduced. Finally we present in Fig.2 an angular distribution for $\pi^+ p \to K^+\Sigma^+$ together with the data from [28]. For this reaction the angular distributions of the existing data show indications of structures which go beyond s- and p-waves (i.e. deviations from a parabola in $\cos\theta$). Nevertheless the gross features are still reasonably well reproduced by our calculation.

3.3 Total cross sections for η- and K-photoproduction

In Fig.3, we show total cross sections for η-photoproduction, $\gamma p \to \eta p$, together with the data of [6] (MAMI) and [7] (ELSA). As expected the total cross section is dominated here by the s-wave multipole E_{0+}, whose value at threshold is $E_{0+,th}^{(\eta p)} = (9.8 + 12.8\,i) \cdot 10^{-3} m_\pi^{-1}$. Again these large cross sections arise from coupled channel dynamics (forming a $K\Sigma$ quasi-bound state) with no explicit $S_{11}(1535)$ introduced. Furthermore, we show in Fig.3 the total cross sections for K^+-photoproduction $\gamma p \to K^+\Lambda, K^+\Sigma^0$ together with the recent data [9] measured by the SAPHIR collaboration at ELSA. In the channel $\gamma p \to K^+\Lambda$ a strong s-wave cusp effect is visible at the $K\Sigma$-threshold. In fact the data show a structure around $E_\gamma = 1.05$ GeV which is consistent with this interpretation. The (complex) electric dipole amplitude at threshold has the value $E_{0+,th}^{(K^+\Lambda)} = (-2.7 - 3.1\,i) \cdot 10^{-3} m_\pi^{-1}$. Above $E_\gamma = 1.2$ GeV the p-wave multipole amplitudes $(E_{1+}, M_{1\pm})$ become very important in order to reproduce the energy dependence of the $K^+\Lambda$-data. The same features apply to the channel $\gamma p \to K^+\Sigma^0$, where $E_{0+,th}^{(K^+\Sigma^0)} = (3.8 + 1.5\,i) \cdot 10^{-3} m_\pi^{-1}$. As in our previous work [1] there is a some overestimation near threshold in $\gamma p \to K^+\Sigma^0$. In both cases there appears in the data an enhancement around $E_\gamma \simeq 1.5$ GeV (corresponding to $\sqrt{s} = 1.9$ GeV). It may be due to a nucleon resonance which couples to $K\Lambda$ and $K\Sigma$. Our coupled channel calculation can generate only non-resonant background amplitudes in p-waves and is thus not able to describe this enhancement if it is due to a resonance. Finally, we show results for neutral kaon-photoproduction, $\gamma p \to K^0\Sigma^+$, together with the recently measured total cross section data from ELSA [10]. The calculation gives an electric dipole amplitude at

threshold of $E_{0+,th}^{(K^0\Sigma^+)} = (1.6 + 1.6\,i) \cdot 10^{-3} m_\pi^{-1}$. In this channel the p-wave multipoles are completely dominant and we find a fair reproduction of the total cross section data from threshold up to about $E_\gamma = 1.4$ GeV. Note that in comparison to [4] our approach does not have the problem of overpredicting the $\gamma p \to K^0\Sigma^+$ cross section.

Altogether, it is highly non-trivial to generate the pattern of s- and p-wave contributions as shown in Fig.3 with its distinct features in each channel, given all the additional constraints from pion-induced η- and K-production (Fig.1).

3.4 Differential cross sections for η- and K-photoproduction

In Fig.4, we show some typical examples of angular distributions of differential cross sections for η- and K-photoproduction. In the case $\gamma p \to p\eta$ the MAMI data [6] display an almost isotropic angular distribution. The small deviations from isotropy at the higher energies $E_\gamma \simeq 0.8$ GeV can be explained in our calculation by the interference term of the large s-wave with the small p-wave multipoles. However, this good agreement does not necessarily imply that p-waves are indeed present in $\gamma p \to \eta p$ below $E_\gamma = 0.8$ GeV since higher multipoles (d-waves) could cause a similar effect. The angular distributions for $\gamma p \to K^+\Sigma^0$ of the recent ELSA data [9] are reasonably well reproduced from threshold up to $E_\gamma \simeq 1.7$ GeV in our coupled channel calculation. Similar features apply to the reaction $\gamma p \to K^+\Lambda$ for $E_\gamma \leq 1.4$ GeV, although the measured angular distributions [9] are (within errorbars) close to a straight line (in $\cos\theta$) whereas the calculated ones have larger curvature ($\cos^2\theta$-term). Finally, we show in Fig.4 two angular distributions of the differential cross section for $\gamma p \to K^0\Sigma^+$ together with the recently measured ELSA-data [10]. For photon energies up to $E_\gamma \simeq 1.4$ GeV the overall behavior of these data can be well described by our coupled channel calculation. In summary, we find in fact that the (recently measured) angular distributions for η- and K-photoproduction are better reproduced than those for pion-induced processes (section 3.2).

3.5 Polarization observables for η- and K-photoproduction

In Fig.5, we show characteristic examples of polarization observables for η- and K-photoproduction. The calculated target asymmetry for $\gamma p \to \eta p$ is positive and grows steadily with photon energy. The existing ELSA data [12] for A_t are instead oscillating about zero and do not exceed magnitudes of 0.2. For the photon asymmetry Σ_γ the situation is opposite. The calculation gives small and negative values whereas the recent GRAAL measurements [11] have found positive photon asymmetries which grow with energy. Since these features of the polarization data could in principle be explained by s- and p-wave multipoles, it appears that the real and imaginary parts of the three p-wave multipoles ($E_{1+}, M_{1\pm}$) for $\gamma p \to \eta p$ are not given correctly by the present calculation, whereas their magnitudes are satisfactory. Unlike the total and differential cross sections, polarization observables are very sensitive to the interference pattern of the complex multipole amplitudes.

Finally, we show recoil polarizations Π_r for K^+- and K^0-photoproduction. In the case $\gamma p \to K^+\Sigma^0$ the trend of the recent ELSA data [9] is roughly reproduced by the calculation. The oscillations of Π_r for $\gamma p \to K^+\Lambda, K^0\Sigma^+$ [9, 10] can, however, not be explained. Clearly, the polarization observables cannot yet be satisfactorily understood in our approach which is strongly constrained by a large amount of additional empirical information. This may point to the importance of dynamical effects beyond non-resonant background amplitudes. To our knowledge there is at present no model (with a reasonably small number of adjustable parameters) which can simultaneously explain the huge amount of data considered here.

4 Summary

In this work we have extended our non-perturbative chiral SU(3) coupled channel approach to pion- and photon-induced η- and K-production off protons by including all strong and electromagnetic p-wave multipoles. The p-wave amplitudes of the next-to-leading order SU(3) chiral meson-baryon Lagrangian are identified with a coupled channel potential which is iterated to infinite orders in a separable Lippmann-Schwinger equation. Seven adjustable parameters $(g_{D,F,0,1}, h_{D,F,1})$ enter in the strong interaction p-wave amplitudes. The further step to η- and K-photoproduction does not introduce any additional free parameters since the baryon magnetic moments are well known. The latter are important in order to be able to generate large $M_{1\pm}$-multipoles for K-photoproduction as required by the data. The drawback of the model at this stage is that the elastic πN-channel is not yet handled with sufficient accuracy.

Altogether, one finds a good reproduction of the total cross sections for pion- and photon-induced η- and K-production. The gaps left in our previous work [1] where only s-waves have been considered are filled by the p-waves of the coupled channel approach. This requires a highly non-trivial pattern of relative weights of s- and p-wave contributions. The angular distributions for η- and K-photoproduction are fairly well reproduced throughout. However, there remain some discrepancies in the angular distributions of pion-induced production and particularly in the polarization observables of photoproduction. These may point towards the importance of other dynamics or the need to include further channels (such as the η' with its close link to the axial U(1) anomaly in QCD). Work along these lines is in progress, together with a more accurate treatment of the elastic πN-channel.

Acknowledgments

We are grateful J. Didelez and S. Goers for very valuable information on the experimental data.

Appendix A

Here we give the explicit expressions for the p-wave coupling strengths $C_{ij}^{1\mp}$ in the relevant meson-baryon channels. The channels $|\pi N\rangle$, $|\eta N\rangle$, $|K\Lambda\rangle$, $|K\Sigma\rangle$ with total isospin $I = 1/2$ and $|\pi N\rangle$, $|K\Sigma\rangle$ with total isospin $I = 3/2$ are labeled with indices $1, \ldots, 6$, in this order.

a) $\underline{p_{1/2}\text{-channels:}}$

$$
\begin{aligned}
C_{11}^{(1-)} &= -\frac{1}{2M_0} - \frac{1}{3}(g_D + g_F + 2g_0 + 4h_D + 4h_F) + 2(D+F)^2 P_{\pi\pi}\,, \\
C_{12}^{(1-)} &= -\frac{1}{3}(g_D + g_F) + (D+F)(3F-D) P_{\pi\eta}\,, \\
C_{13}^{(1-)} &= \frac{3}{8M_0} + \frac{1}{6}(g_D + 3g_F + 2h_D + 6h_F) - \frac{1}{4}(D^2 + 14DF + 9F^2) P_{\pi K}\,, \\
C_{14}^{(1-)} &= -\frac{1}{8M_0} + \frac{1}{6}(g_D - g_F - 2g_1 + 4h_1 + 2h_D - 2h_F) + \frac{1}{12}(25D^2 + 6DF - 39F^2) P_{\pi K}\,, \\
C_{22}^{(1-)} &= \frac{1}{9}(3g_F - 5g_D - 6g_0) + \frac{1}{3}(D-3F)^2 P_{\eta\eta}\,, \\
C_{23}^{(1-)} &= \frac{3}{8M_0} + \frac{1}{18}(12h_1 + 6h_D + 18h_F - g_D - 3g_F - 6g_1) + \frac{1}{12}(5D^2 + 6DF - 27F^2) P_{\eta K}\,, \\
C_{24}^{(1-)} &= \frac{3}{8M_0} + \frac{1}{6}(g_D - g_F - 6h_D + 6h_F) + \frac{1}{4}(10DF - D^2 - 9F^2) P_{\eta K}\,,
\end{aligned}
$$

$$
\begin{aligned}
C_{33}^{(1-)} &= -\frac{1}{9}(5g_D+6g_0+6h_D)+\frac{1}{3}(D^2+3DF+9F^2)P_{KK}\,,\\
C_{34}^{(1-)} &= \frac{1}{3}(2h_D-g_D)+(3F^2-DF-D^2)P_{KK}\,,\\
C_{44}^{(1-)} &= -\frac{1}{2M_0}+\frac{1}{3}(2g_F-g_D-2g_0+2h_D-4h_F)+(2D^2-5DF+2F^2)P_{KK}\,,\\
C_{55}^{(1-)} &= \frac{1}{4M_0}+\frac{1}{3}(2h_D+2h_F-g_D-g_F-2g_0)+\frac{1}{2}(D+F)^2P_{\pi\pi}\,,\\
C_{56}^{(1-)} &= \frac{1}{4M_0}+\frac{1}{3}(g_F-g_D-g_1+2h_1-2h_D+2h_F)+\frac{1}{6}(3F^2-6DF-D^2)P_{\pi K}\,,\\
C_{66}^{(1-)} &= \frac{1}{4M_0}+\frac{1}{3}(2h_D+2h_F-g_D-g_F-2g_0)+\frac{1}{2}(D+F)^2P_{KK}\,. \qquad (30)
\end{aligned}
$$

b) $\underline{p_{3/2}\text{-channels:}}$

$$
\begin{aligned}
C_{11}^{(1+)} &= \frac{1}{3}(2h_D+2h_F-g_D-g_F-2g_0)+\frac{1}{2}(D+F)^2P_{\pi\pi}\,,\\
C_{12}^{(1+)} &= -\frac{1}{3}(g_D+g_F)+\frac{1}{2}(D+F)(D-3F)P_{\pi\eta}\\
C_{13}^{(1+)} &= \frac{1}{6}(g_D+3g_F-h_D-3h_F)+D(F-D)P_{\pi K}\,,\\
C_{14}^{(1+)} &= \frac{1}{6}(g_D-g_F-2g_1-2h_1-h_D+h_F)+\frac{1}{3}(D^2-3DF+6F^2)P_{\pi K}\,,\\
C_{22}^{(1+)} &= \frac{1}{9}(3g_F-5g_D-6g_0)-\frac{1}{6}(D-3F)^2P_{\eta\eta}\,,\\
C_{23}^{(1+)} &= -\frac{1}{18}(6h_1+3h_D+9h_F+g_D+3g_F+6g_1)-D\Big(F+\frac{D}{3}\Big)P_{\eta K}\,,\\
C_{24}^{(1+)} &= \frac{1}{6}(g_D-g_F+3h_D-3h_F)+D(F-D)P_{\eta K}\,,\\
C_{33}^{(1+)} &= \frac{1}{9}(3h_D-5g_D-6g_0)-\frac{1}{6}(D-3F)^2P_{KK}\,,\\
C_{34}^{(1+)} &= -\frac{1}{3}(h_D+g_D)+\frac{1}{2}(D+F)(D-3F)P_{KK}\,,\\
C_{44}^{(1+)} &= \frac{1}{3}(2g_F-g_D-2g_0-h_D+2h_F)+\frac{1}{2}(D+F)^2P_{KK}\,,\\
C_{55}^{(1+)} &= -\frac{1}{3}(h_D+h_F+g_D+g_F+2g_0)-(D+F)^2P_{\pi\pi}\,,\\
C_{56}^{(1+)} &= \frac{1}{3}(g_F-g_D-g_1-h_1+h_D-h_F)+\frac{1}{3}(D^2+6DF-3F^2)P_{\pi K}\,,\\
C_{66}^{(1+)} &= -\frac{1}{3}(h_D+h_F+g_D+g_F+2g_0)-(D+F)^2P_{KK}\,. \qquad (31)
\end{aligned}
$$

The abbreviation $P_{\phi\phi'}$ in eqs.(7,8) stands for

$$
P_{\phi\phi'}=\frac{1}{6E_\phi E_{\phi'}}\Big(E_\phi+E_{\phi'}+\frac{2E_\phi E_{\phi'}+m_\phi^2+m_{\phi'}^2}{2M_0}\Big)\,. \qquad (32)
$$

One makes the following observations. The SU(3) Weinberg-Tomozawa meson-baryon contact vertex contributes only to the $p_{1/2}$-potentials a relativistic correction proportional to $1/M_0$. The s-channel pole diagrams (i.e. meson absorption and subsequent emission on the baryon line) contribute of course only to the $p_{1/2}$-potentials, namely with strength $3P_{\phi\phi'}$.

The contributions of the (crossed) u-channel pole diagrams to the $p_{3/2}$-potentials differs by a factor -2 from the ones to the $p_{1/2}$-potentials (i.e. $-2P_{\phi\phi'}$ versus $P_{\phi\phi'}$). Note that we have used the freedom to add higher order terms in the small momentum expansion in order to arrive at the fully symmetric expression for $P_{\phi\phi'}$. Finally, there are the p-wave contact terms in eq.(1) which generate the contributions proportional to $g_{D,F,0,1}$ and $h_{D,F,1}$.

References

[1] N. Kaiser, T. Waas and W. Weise, *Nucl. Phys.* **A612** (1997) 297.

[2] N. Kaiser, P.B. Siegel and W. Weise, *Nucl. Phys.* **A594** (1995) 325; *Phys. Lett.* **B362** (1995) 23.

[3] R.A. Adelseck and B. Saghai, *Phys. Rev.* **C42** (1990) 108; **C45** (1992) 2030.

[4] T. Mart, C. Bennhold and C.E. Hyde-Wright, *Phys. Rev.* **C51** (1995) R1074.

[5] Ch. Sauermann, B.L. Friman and W. Nörenberg, *Phys. Lett.* **B341** (1995) 261.

[6] B. Krusche *et al.*, *Phys. Rev. Lett.* **74** (1995) 3736.

[7] B. Schoch, *Prog. Part. Nucl. Phys.* **34** (1995) 43.

[8] M. Bockhorst *et al.*, *Z. Phys.* **C63** (1994) 37.

[9] M.Q. Tran *et al.* (SAPHIR Collaboration), *Phys. Lett.* **B445** (1998) 20.

[10] S. Goers et al. (SAPHIR collaboration), *Phys. Lett.* **B464** (1999) 331.

[11] J. Ajaka *et al.*, *Phys. Rev. Lett.* **81** (1998) 1797.

[12] A. Bock *et al.*, *Phys. Rev. Lett.* **81** (1998) 534.

[13] M.E. Sadler, (Crystal Ball Collaboration), *πN Newsletter* **13** (1997) 123.

[14] G. Müller and U.G. Meißner, *Nucl. Phys.* **B492** (1997) 379.

[15] B. Borasoy and U.G. Meißner, *Ann. Phys. (NY)* **254** (1997) 232.

[16] S. Steininger and U.G. Meißner, *Nucl. Phys.* **B499** (1997) 359.

[17] W.M. Kloet and B. Loiseau, *Eur. Phys. J.* **A1** (1998) 337.

[18] R.D. Baker *et al.*, *Nucl. Phys.* **B141** (1978) 29.

[19] J. Gasser, H. Leutwyler and M.E. Sainio, *Phys. Lett.* **B253** (1991) 252.

[20] E. Oset and A. Ramos, *Nucl. Phys.* **A635** (1998) 99.

[21] Review of Particle Properties, *Phys. Rev.* **D45** (1992).

[22] A. Baldini, *et al.*, in Landolt-Börnstein, Vol. 12a, (Springer, Berlin, 1988).

[23] I. Dadic *et al.*, *Physica Scripta* **58** (1998) 15.

[24] R.M. Brown *et al.*, *Nucl. Phys.* **B153** (1979) 89.

[25] M.L. Good and R.R. Kofler, *Phys. Rev.* **183** (1969) 1142.

[26] R.D. Baker *et al.*, *Nucl. Phys.* **B145** (1978) 402.

[27] R.D. Baker *et al.*, *Nucl. Phys.* **B141** (1978) 29.

[28] D.J. Candlin *et al.*, *Nucl. Phys.* **B226** (1983) 1.

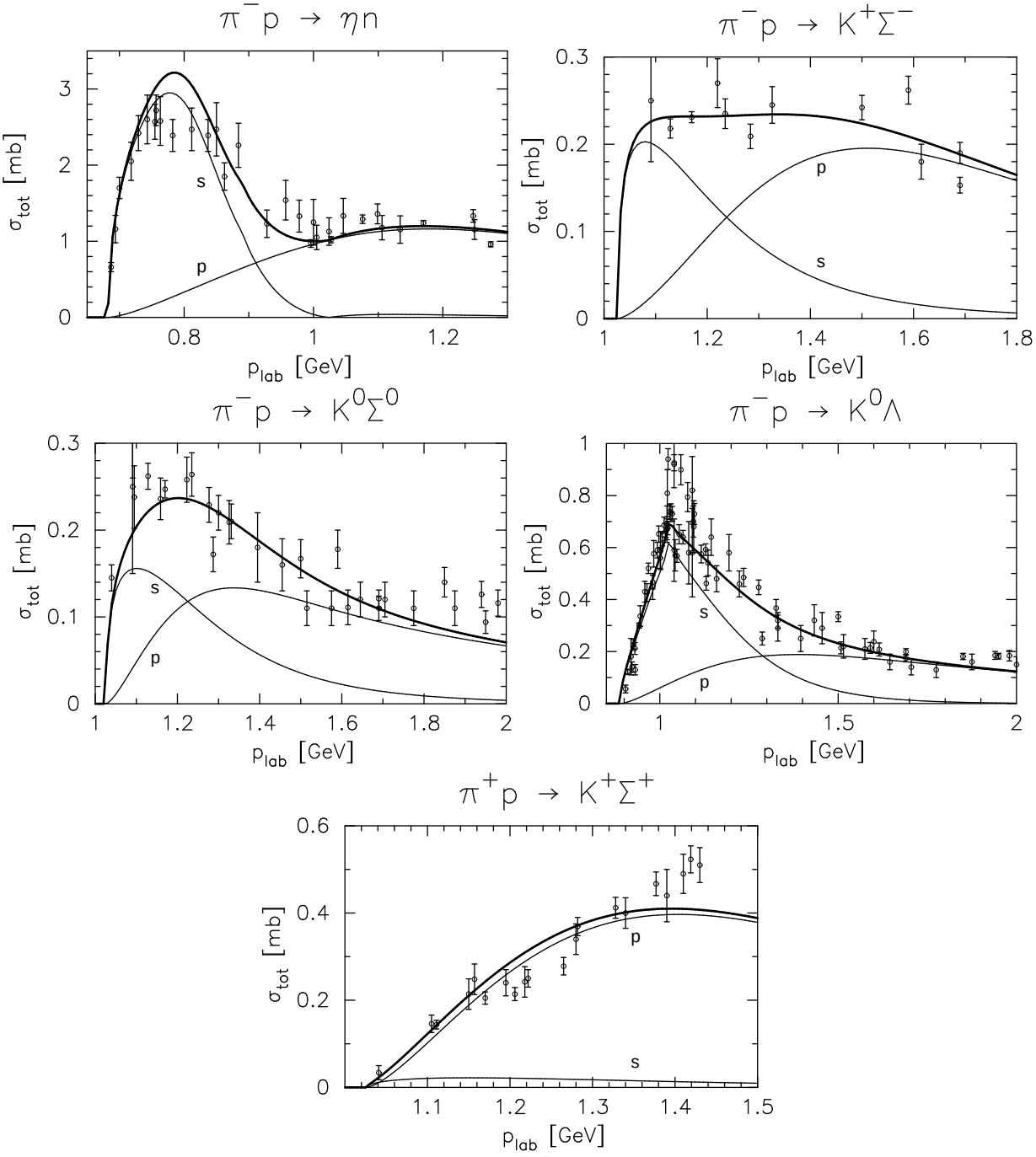

Figure 1: Total cross sections for pion-induced η- and K-production as a function of the pion laboratory momentum. The s- and p-wave contributions are shown separately. The data are taken from the compilation [22].

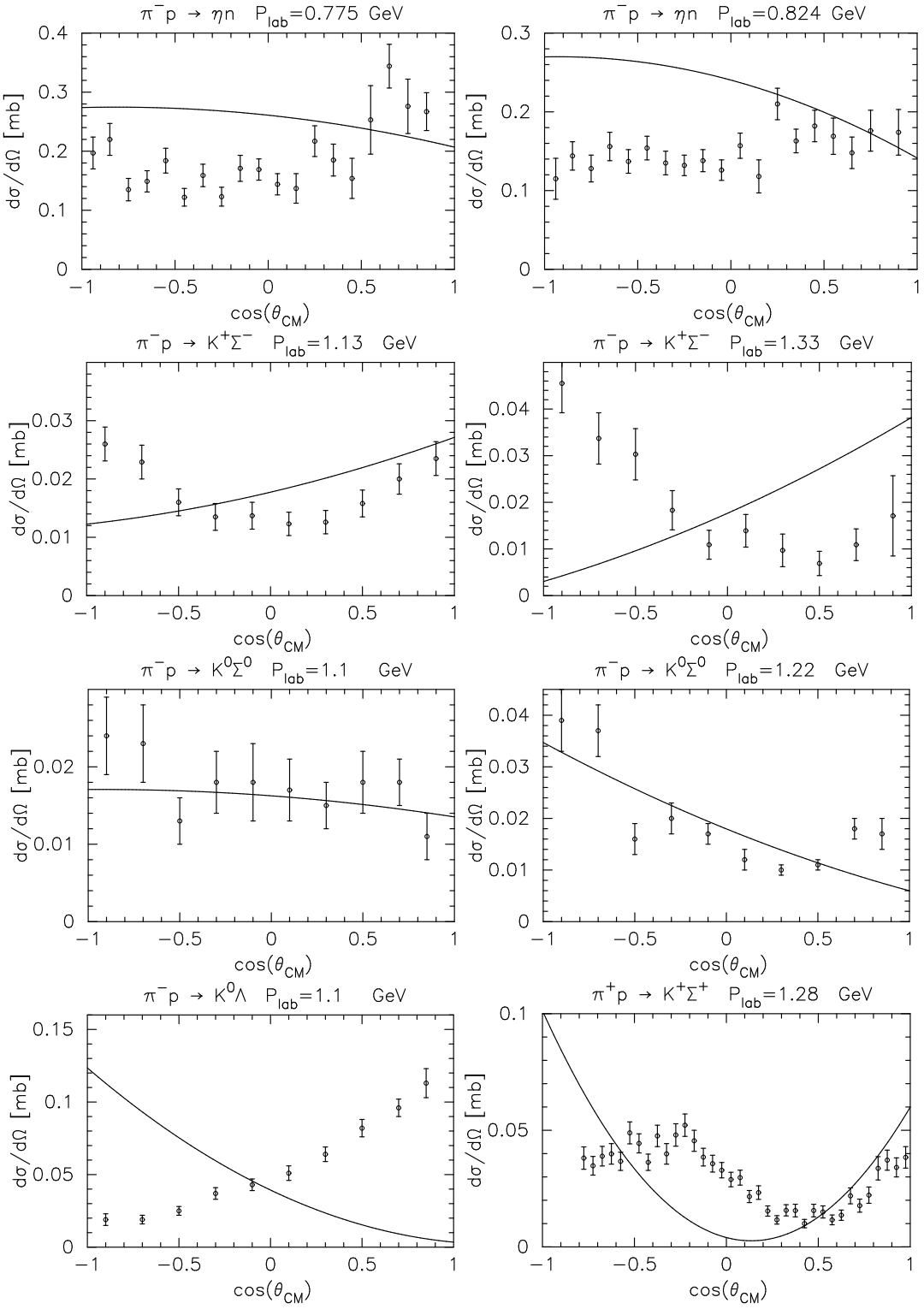

Figure 2: Angular distributions of differential cross sections for pion-induced η- and K-production as a function of $z = \cos\theta$. The data are taken from [24, 25, 26, 27, 28].

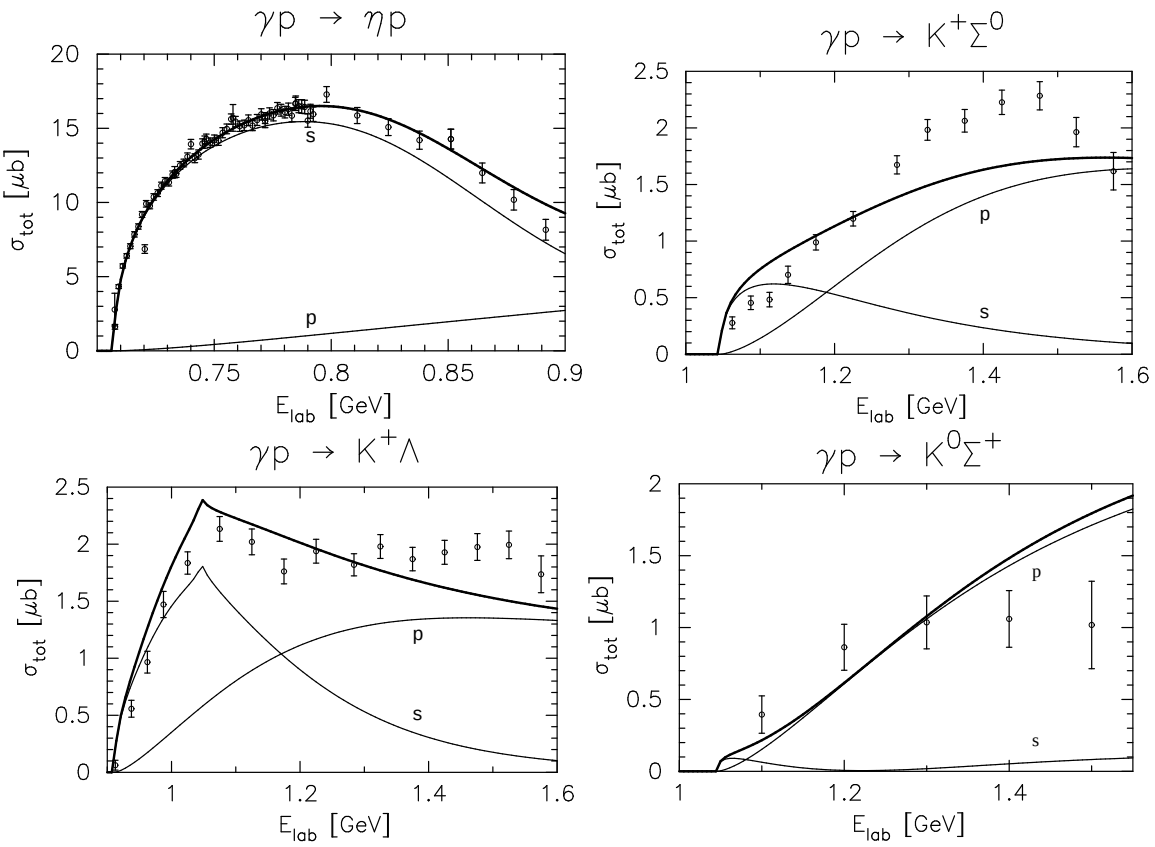

Figure 3: Total cross sections for η- and K-photoproduction as a function of the photon laboratory energy. The s- and p-wave contributions are shown separately. The data are taken from [6, 7, 9].

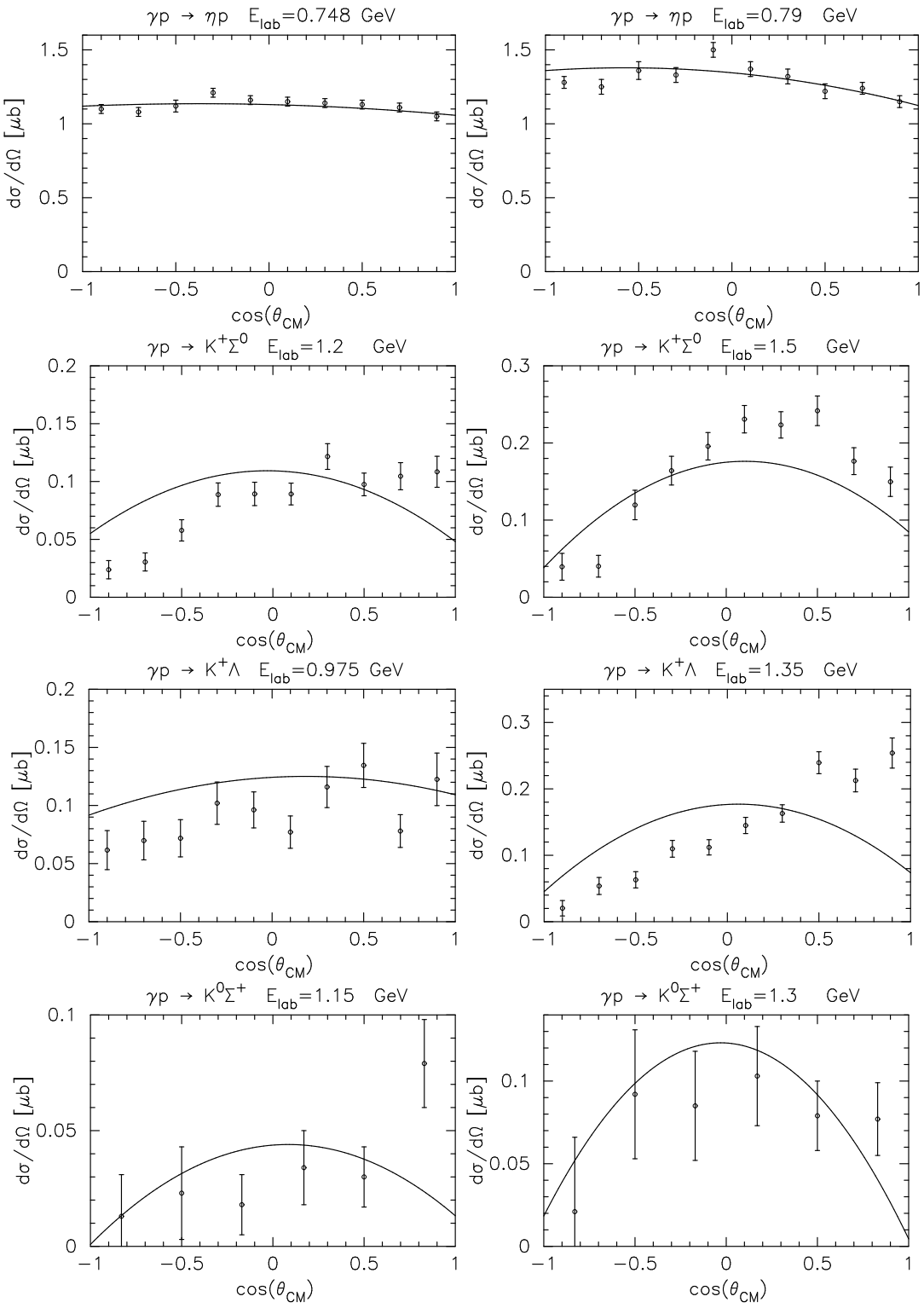

Figure 4: Angular distributions of differential cross sections for η- and K-photoproduction as a function of $z = \cos\theta$. The data are taken from [6, 9].

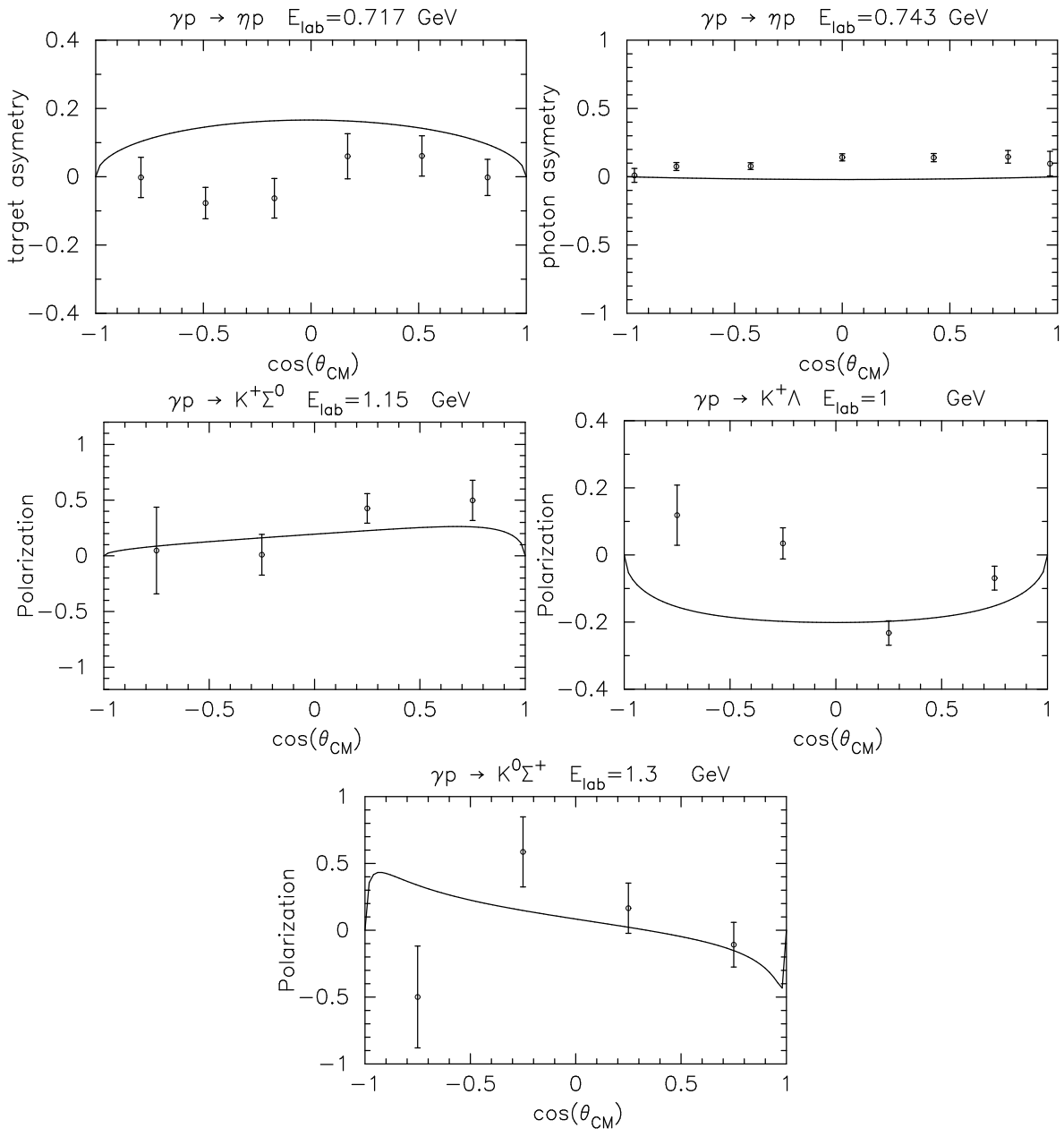

Figure 5: Polarization observables for η- and K-photoproduction as a function of $z = \cos\theta$. The data are taken from [9, 10, 11, 12].